Convergence
A Journal for Young Researchers

ORIGINAL RESEARCH

Received: 5-1-26; Accepted: 6-9-26;
Managing Editor: Jonas Katona;
Action Editor: Christa Caggiano

Investigation of Histone Modification and Alternative Splicing Association in Neural and Non-Neural Tissues

Ryota Watanabe

Crimson Global Academy, Remote

Abstract

Pre-mRNA splicing is a complex and vital process utilized in eukaryotes. Histone modifications are known to affect splicing through recruiting factors to the nascent pre-mRNA. They also influence splicing outcomes through modulating the elongation rate of RNA Polymerase II by altering the degree of chromatin compaction. We hypothesized that the H3K36me3 histone modification in genes known to be neurally regulated would be enriched compared to non-neural tissues, as a potential contributor to tissue-specific splicing. Using publicly available ChIP-Seq and RNA-Seq data from embryonic and postnatal mouse tissues, we analyzed the differences in H3K36me3 signals between brain and non-neural tissues for select genes known to play an important role in brain function. We found that exon inclusion was associated with H3K36me3 across tissues in the Bin1 gene, although the correlation was less pronounced in other genes. Furthermore, we observed that changes in H3K36me3 during brain development were associated with changes in alternative splicing patterns at the same developmental time point. By identifying these associations, we postulate that H3K36me3 could serve as a key determinant of alternative splicing outcomes.

Keywords: H3K36me3, alternative splicing, histone modifications, chromatin, epigenetics, co-transcriptional splicing, ChIP-seq, RNA-seq, neural tissue, mouse brain development

1. Introduction

DNA is the genetic material which universally codes for the proteins of almost all organisms. A singular diploid cell in the human body contains six billion base pairs, spanning two meters wide end-to-end (Piovesan et al., 2019). To compact it for packaging within the 10 micrometer nucleus, the DNA is wrapped around an octamer of positively charged proteins known as histones, which, when combined with associated RNAs, form chromatin (Georgopoulos, 2017). Chromatin can be modified in various ways, such as DNA methylation and histone modifications. Histone modifications are known to affect key properties of the chromatin, such as DNA accessibility, altering the extent to which proteins and transcription factors must compete with histones for DNA binding and utilization (Pfluger & Wagner, 2007). For example, accessibility was decreased by H3K27 methylation and increased by acetylation or H3K36 methylation (Bannister & Kouzarides, 2011; Greer & Shi, 2012).

Alternative splicing is the process of producing multiple distinct mRNAs (isoforms) from the same pre-mRNA via joining exons (coding regions) in different combinations, used by higher eukaryotes for increased transcriptomic and proteomic diversity (Wright et al., 2022). It is mediated by splicing factors that guide the spliceosome, a complex assembled along the introns of small ribonuclear proteins, to the splice sites to cut out introns (non-coding regions) (Marasco & Kornblihtt, 2023). Alternative splicing preferentially occurs at suboptimal splice sites, giving rise to varying proportions of the variants, but splicing factors can bind to certain sequences to influence which splice site is used (Marasco & Kornblihtt, 2023). This process is vital to eukaryotes, and its misregulation was implicated in cancers and neurological disorders (Marasco & Kornblihtt, 2023).

Recent studies illuminated strong connections between histone modifications and alternative splicing (Yustis et al., 2024). The research in post-translational modifications, chromatin state, and elongation speed's ability to directly influence splicing has arisen due to evidence that splicing occurs simultaneously to transcription, in other words, co-transcriptionally (Leung et al., 2019a) (Figure 1A)

Two models are prominent as the current consensus of how the chromatin landscape shapes splicing outcome: the recruitment and the kinetic model. The recruitment model described chromatin and its modifications' interactions with splicing factors during co-transcriptional splicing (Luco et al., 2011; Yustis et al., 2024). The kinetic model proposed that the elongation rate of RNA Polymerase II (RNAP II) altered splice site selection and spliceosome assembly by modulating the availability of splice sites (Yustis et al., 2024). Histone modifications that induce chromatin compaction could also affect the elongation rate, leading to changes in splicing outcomes (de la Mata et al., 2003). Mechanistic models for particular modifications, such as H3K36me3, have been found, where they can regulate splicing through a chromatin reader protein, such as MRG15, which can then recruit splicing factors, such as polypyrimidine tract-binding protein (Figure 1B) (Luco et al., 2010). While the associations between histone modifications and alternative splicing in the brain are well characterized, as the organ with a high frequency of alternative splicing in higher eukaryotes, the significance of the specific gene splicing of histone modifications and their changes across non-neural tissues and developmental phases is underexplored.

H3K36me3 was chosen in this study because it had an experimentally proven role in influencing RNA splicing and an outlined mechanism (Luco et al., 2010). Additionally, the chromodomain protein Eaf3 has been established to link H3K36me3 and the spliceosome for co-transcriptional splicing (Leung et al., 2019b). Although other modifications had

demonstrated enrichment in spliced exon regions and associations with alternative splicing, a computational study investigating histone modifications between IMR90 and H1 cells found H3K36me3 and H3K79me1 to be the only modifications clearly correlated to alternative splicing (Shindo et al., 2013). Moreover, as H3K36me3, in particular, was also strongly associated with half the alternatively spliced events that change upon human embryonic stem cell differentiation, H3K36me3 was chosen so that tissue-specific and developmental correlations would be more grounded (Xu et al., 2018).

The genes analyzed in this study were manually selected such that all four genes chosen had known neurally regulated splicing events, involvement in neurological conditions, and susceptibility to epigenetic modification. This was verified by referring to the list provided in previous literature (Irimia et al., 2014). Specifically, Bridging Integrator 1 (Bin1, NM_001083334) was a neurally regulated gene with functions including regulating endocytosis, which has isoforms relevant to Alzheimer's disease, as well as being affected by DNA methylation (De Jager et al., 2014). Bin1 was also a tumour suppressor that was inactivated through attenuation or mis-splicing in human cancers. Its inactivation could particularly increase the likelihood of lung cancer (Chang et al., 2007). Myocyte enhancer factor 2A (Mef2a, NM_001291192) was a transcription factor that was typically expressed in the heart and neural cells, which could be affected by certain histone modifications, such as acetylation (Passier et al., 2000; Sharma et al., 2014). The aberrant S-nitrosylation (SNO)-MEF2A/TLX cascade was reported to negatively regulate adult neurogenesis in Alzheimer's disease (Okamoto et al., 2014).

Clathrin light chain B (Cltb, NM_028870) was shown to connect endocytic machinery to the cytoskeleton by binding Hip1/R, which in turn binds to actin. It is predicted to be involved in clathrin-dependent endocytosis and could similarly be affected by histone modification profiles (Das et al., 2021a; Forn et al., 2013). CLTB was abnormally distributed in the hippocampi of patients with Alzheimer's and was upregulated in mouse hippocampal models with Alzheimer's (Nakamura, 1994). It was also present in increased amounts in the neuronal perikarya of Pick's disease patients compared to healthy patients (Nakamura et al., 1994). Pyruvate kinase, muscle (Pkm, NM_011099), was involved in canonical glycolysis and was shown to be influenced by H3K36me3 (Luco et al., 2010). Splicing preference for the downstream mutually exclusive exon forms the isoform Pkm2 that was found in elevated levels in postmortem Alzheimer's disease mouse brains and has been implicated in its pathology (Zhang et al., 2025). It could also promote tumour growth (Lin et al., 2021). The selection criteria were designed to ensure that the genes are alternatively spliced before comparing them across tissues. Furthermore, it could increase the probability that H3K36me3 can directly or indirectly regulate gene splicing, rather than merely correlating with it, although it will still naturally require wet lab experimentation to test any associations.

In this study, we aimed to investigate the extent to which the histone modification H3K36me3 acted as a tissue-specific splicing regulator, examining its level of presence in exons that are distinctly spliced across tissues. An additional objective was to determine if H3K36me3 could be significant for developmental differences in exon inclusion percentages to assess its potential impacts on development.

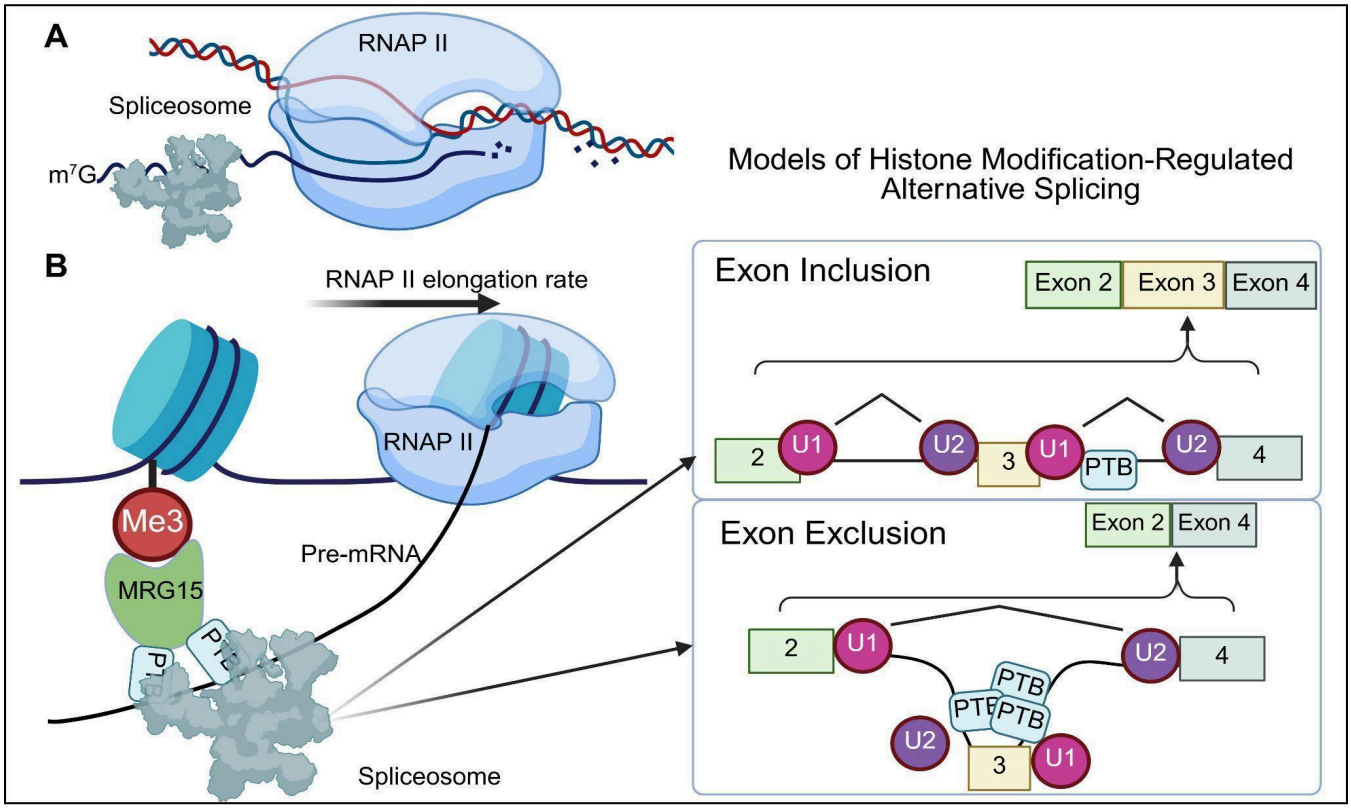

Figure 1: Co-transcriptional splicing and models for histone modification-regulated alternative splicing.

Note: **(A)** A schematic figure illustrating how the RNA Polymerase II (RNAP II) undergoes elongation simultaneously to splicing by the spliceosome, after the m7G cap has been bound. **(B)** A schematic figure depicting the effects of chromatin states on differential splicing outcome through affecting RNAP II elongation speed and chromatin adaptors. H3K36me3 is shown here to be interacting with the chromatin adaptor protein MORF-related gene 15 (MRG15), which then recruits the polypyrimidine tract binding protein (PTB), adapted from (Luco et al., 2010). Subsequently, its location-dependent splicing outcomes are illustrated on the right, with the potential mechanisms. Adapted from (Chou et al., 2000). Figure generated using BioRender.

2. Methodology

2.1. Epigenome browser visualisation of Tabula Muris and ENCODE data

UCSC Genome Browser was used to visualise the publicly available Tabula Muris single-cell (Fluorescence-Activated Cell Sorting (FACS) performed cells sequenced with SmartSeq2 protocol) RNA-Seq data and ENCODE 3 project's Histone Modification ChIP-Seq data from two biological replicates generated by the ENCODE consortium in the Mus musculus

genome (December 2011 (GRCm38/mm10), GCA_000001635.2) (ENCODE Project Consortium, 2012; Perez et al., 2025; Schaum et al., 2018). Although many other modifications, such as H3K9ac and H3K27me3, had previously demonstrated effects on alternative splicing, they were not focused on here due to the scope of this study. (Agirre et al., 2021).

The H3K36me3 data from mice of age postnatal 0 (P0), the oldest available (out of E10.5, E11.5, E12.,5 E13.5, E14.5, E15.5, E16.5, and P0), were used to understand the relationship between histone modifications and alternative splicing during development. Additionally, the signal from embryonic 14 (E14) mice was also quantified to complement the Cortexa data discussed later. We analyzed the H3K36me3 signal ±200 bp from the intron-exon boundaries, which we decided upon from past literature (Agirre et al., 2021; Shindo et al., 2013). The tissues that the neuronal cell population was compared against were manually selected by observing if their expression levels were comparable to those of the neuron. Specifically, tissues were used if their flanking exons had an expression signature value of at least 10 % of the neuron's expression, to ensure that any differences in the splicing could not simply be attributed to the difference in expression. However, some tissues with RNA-Seq data could not be utilized for analysis because the ENCODE dataset employed only contains 12 tissues.

2.2. Measuring developmental exon inclusion percentages

A Cortexa database was used to analyze the changes in exon inclusion percentage in the cerebral cortex in mice with age (Weißbach et al., 2024). We searched the gene names "Bin1", "Pkm", "Cltb", and "Mef2a", which had the splicing events recorded. Although the coordinates of the splicing events in Cortexa did not exactly match those in the GENCODE VM23 Transcript set used in the UCSC Browser, the corresponding events were found as those with equivalent length of the relevant spliced exons.

2.3. Statistical analysis

To quantify the RNA-Seq and ChIP-Seq data, the exact coordinates of the desired region were found using UCSC's Table Browser, with the following configurations: Clade: Mammal, Genome: Mouse, Assembly: Dec. 2011 (GRCm38/mm10), Group: Expression and Regulation, Track: Histone Modifications, Table: H3K36me3 [Selected Organ] [Selected Age]. From the Table Browser, we obtained the summary statistics that included the mean and the standard deviation. Mean and standard deviation values were used to generate graphs on BioRender Graphing (a newly added function to the visualization tool). We then performed unpaired two-tailed t-tests with alpha< 0.05, variances of the samples being homogeneous, and normal distribution using BioRender Graphing.

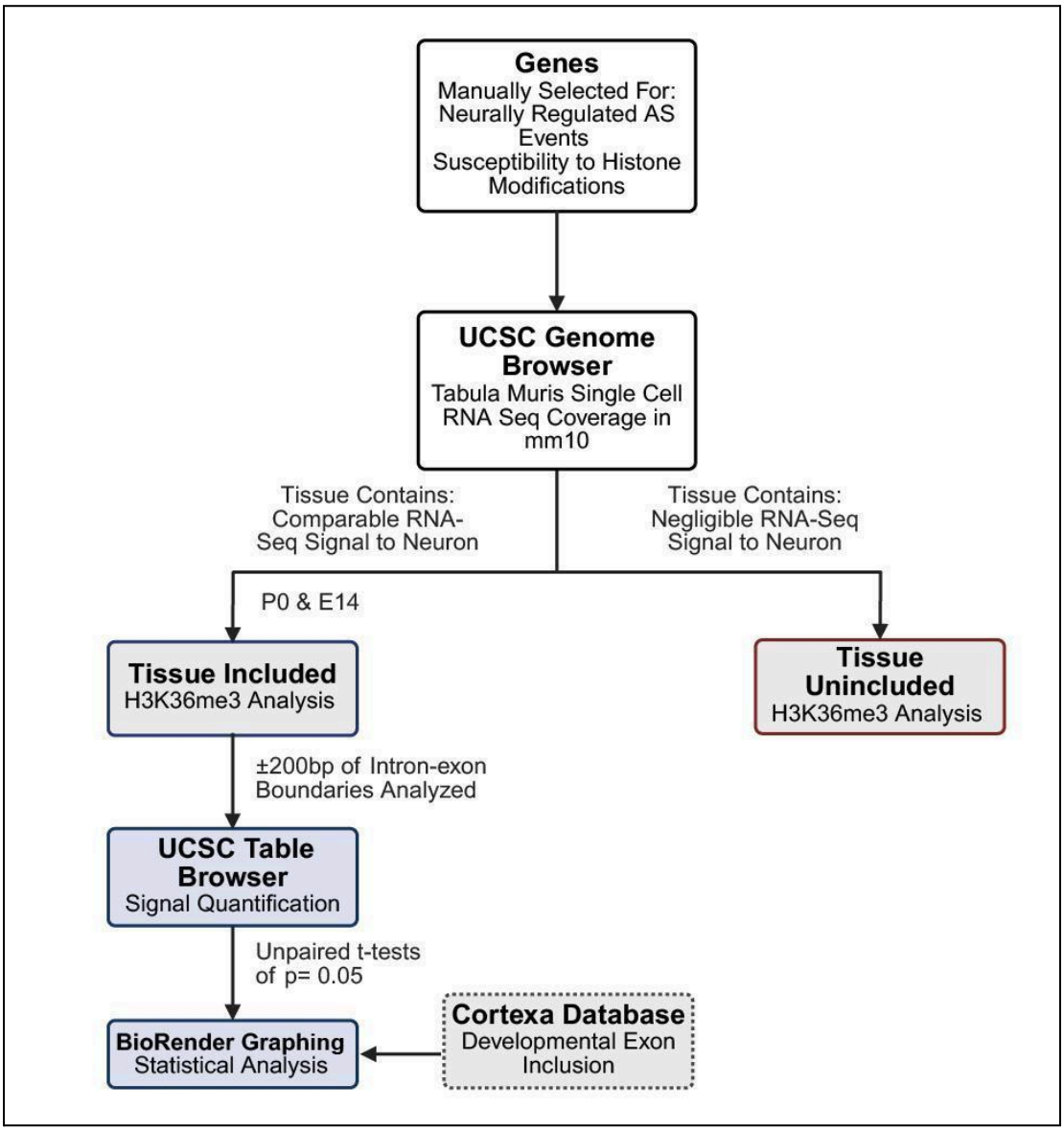

Figure 2: Methodological workflow of this study.

Note: Flowchart depicting the gene selection process, data visualization and analysis methods. The genes were selected based on their susceptibility to alternative splicing in neurons. The tissues were chosen if they had sufficient flanking exon expression signals relative to neurons. The UCSC Table Browser was used to obtain summary statistics, which were analyzed and plotted using the BioRender Graphing tool. The Cortexa database was used to analyze the changes in developmental exon inclusion percentages with changes in H3K36me3.

3. Results

Exon 7 of Bin1 is differentially spliced in neurons

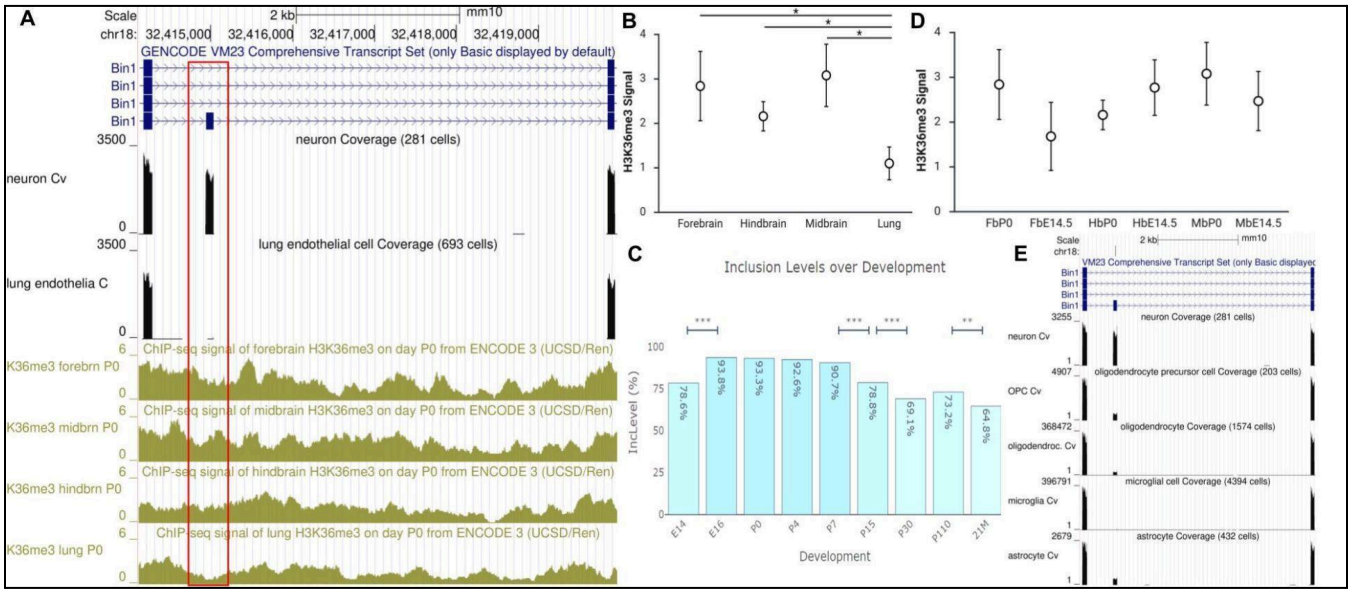

Figure 3: mRNA and H3K36me3 and alternative splicing analyses of Bin1 Exon 7.

Note: **(A)** The RNA-Seq data of neurons (281 cells) and lung endothelia (693 cells), visualized along with the associated tissues' H3K36me3 signals. **(B)** A graph where the circle represents the mean and the tails/error bars represent the standard deviation (SD) of the H3K36me3 signal of the four different tissues. P values: 0.0251 (Forebrain - Lung), 0.0123 (Midbrain - Lung), 0.0208 (Hindbrain - Lung). 495 bases analyzed in (B) and (D). **(C)** The changes in inclusion levels over development, adapted from Cortexa (Weißbach et al., 2024). **(D)** Graph of H3K36me3 signal of the three brain regions (Forebrain - Fb, Midbrain - Mb, Hindbrain - Hb) from Age E14.5 to P0, where the circle represents the mean, and the error bars represent the SD (B and D, quantified region: chr18:32,414,746-32,415,240 | NM_001083334). (FbP0 – FbE14.5: p>0,05), (HbP0 – HbE14.5: p>0,05), (MbP0 – MbE14.5: p>0,05). **(E)** RNA-Seq data of the neuron, OPC, oligodendrocyte, microglia, and astrocyte. Their y-axes are not normalized at the microglia despite its 100-fold greater expression to emphasize the neuron-specific splicing pattern. P-values: * < 0.05, ** < 0.01, *** < 0.001. Graphs without indicated statistical significance indicate a lack of significant differences.

Analysis of Exon 7 of Bin1 revealed differential splicing between neurons and lung endothelia. Exon 7 encodes part of the BAR domain that has been implicated in dynamin regulation and regulation of membrane targeting specificity (Spooner & Dixon, 2025). Both flanking exons were expressed to comparable levels in both neurons and the lung endothelia, while neurons exclusively had exon 7 included. The percentage spliced in (PSI) relative to the average RNA-Seq of its flanking exons for exon 7 was 88.5% and 1.15%, respectively (to 3 significant figures). This was in concordance with findings

suggesting a functional role of exon 7 in controlling the efficiency of neural cell endocytosis by promoting Dnm2 interactions (Ellis et al., 2012). Analyzing the corresponding methylation pattern showed H3K36me3 signatures in the lung near the exon, which were outside of the exon region (quantified in the red box, Fig. 3A), while the midbrain had peaks both near and inside the region. Further quantification of H3K36me3 signal in the region displayed significant differences in H3K36me3 signal between the lung and all three areas of the fore, mid and hindbrain for Bin1, where the signal appeared greater in all areas of the brain. However, among the genes analyzed in this study, Bin1 is the only gene to display significant organ-specific H3K36me3 signals (Fig. 3B). We next asked if Exon 7 is developmentally regulated in the mouse brain. The inclusion level of the exon in the mouse brain increases significantly from E14 to E16 (78.6% to 93.8%, respectively), but not from E16 to P0 (Fig. 3C); however, no significant differences were found between the H3K36me3 signals of the brain samples aged E14.5 to P0 for all three brain regions (Fig. 3D).

There was a limitation to this data, which was that the H3K36me3 data were derived from a bulk assay of many cell types within the tissue, while the RNA-Seq data were cell-specific. Thus, we have included the RNA-Seq data of all the types of brain cells for which the data are accessible in the Tabula Muris tracklist in part E, including the neuron, astrocyte, OPC, microglia, and oligodendrocytes. The splicing patterns were distinct, where neurons had a high degree of inclusion of exon 7, while OPC, astrocytes, and oligodendrocytes had much lower inclusion, and microglia had no observable inclusion. The expression of the gene itself varied widely, with the microglia and oligodendrocytes having much greater RNA-Seq signal than the rest. (Fig. 3E) This was in concordance with past literature on Bin1 (Dourlen et al., 2025).

2.4. Skipping of exon 9 of Mef2a is differentially regulated in neurons

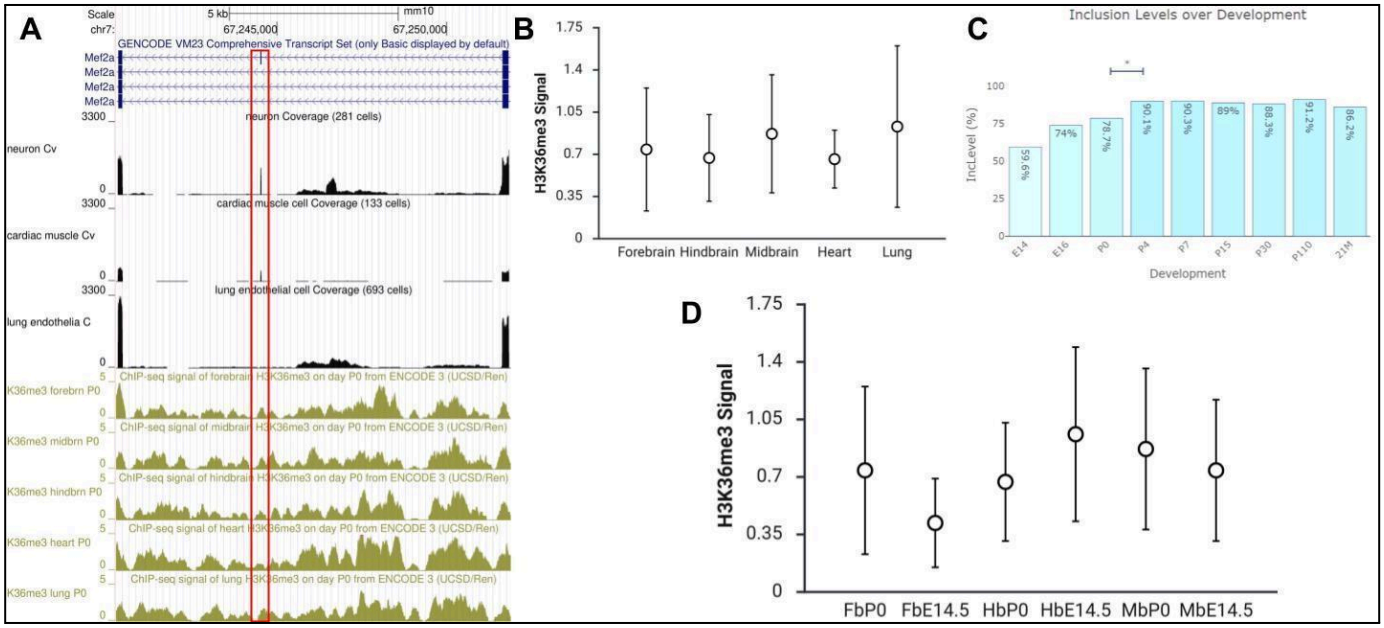

Figure 4: mRNA and H3K36me3 and alternative splicing analyses in Mef2a Exon 9.

Note: **(A)** The RNA-Seq data of neuron (281 cells), cardiac muscle (133 cells), and lung endothelia (693 cells), visualized along with the associated tissues' H3K36me3 signals. **(B)** A graph where the circle represents the mean and the tails/error bars represent the standard deviation (SD) of the H3K36me3 signal of the five different tissues. (Forebrain – Heart, Lung: p>0,05), (Hindbrain – Heart, Lung: p>0,05), (Midbrain – Heart, Lung: p>0,05). 425 bases analyzed in (B) and (D). **(C)** The changes in inclusion levels over development, adapted from Cortexa (Weißbach et al., 2024). **(D)** Graph of H3K36me3 signal of the three brain regions from Age E14.5 to P0, where the circle represents the mean, and the error bars represent the SD (B and D, quantified region: chr7:67,244,319-67,244,743 | NM_001291192). (FbP0 – FbE14.5: p>0,05), (HbP0 – HbE14.5: p>0,05), (MbP0 – MbE14.5: p>0,05). P-values: * < 0.05, ** < 0.01, *** < 0.001. Graphs without indicated significance indicate a lack of significant differences.

Similar to Bin1, Exon 9 of Mef2a also displayed differential splicing between the neuron and the lung endothelia, where the lung exclusively excluded it (PSIs were 67.5% to 2.11%, respectively), while the cardiac muscle was spliced similarly to the neuron (PSI 84.7%). The cardiac muscle is shown for comparison with the neuron. Exon 9's function is unknown, but it was more skipped in patients' hearts with Type 2 diabetes (Nutter et al., 2016). The flanking exons of all the neurons, heart, and lungs were comparably expressed. All quantified regions had small peaks within them, with generally similar H3K36me3 signature patterns across the tissues in the visible areas. (Fig. 4A) Quantification of the regions indicated no significant differences between the H3K36me3 signals of any tissues, where all five tissues had very similar mean signatures. (Fig. 4B) We then asked whether Exon 9 was developmentally regulated in the mouse brain. Although there appeared to be a general trend of increasing exon inclusion, there were no significant differences between E14 and P0, the ages studied. (Fig. 4C) Similarly, we found no significant differences between the H3K36me3 signatures in all three brain regions. (Fig. 4D)

2.5. Exon 5 of Cltb is differentially spliced in neurons and developmentally regulated

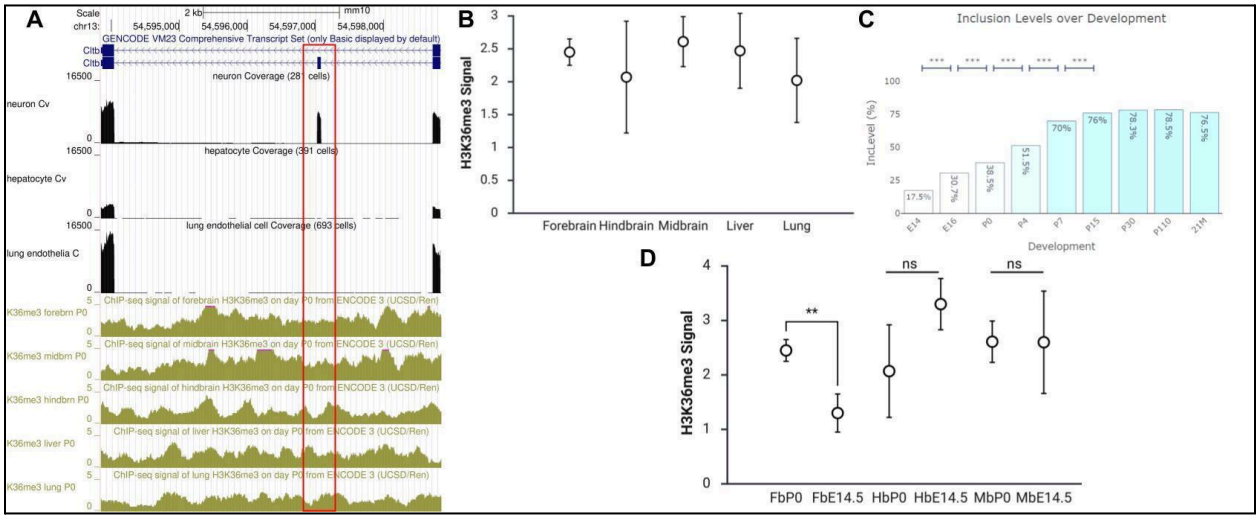

Figure 5: mRNA and H3K36me3 and alternative splicing analyses in Cltb Exon 5.

Note: **(A)** The RNA-Seq data of neuron (28 cells), hepatocyte (391 cells), and lung endothelia (693 cells), visualized along with the associated tissues' H3K36me3 signals. **(B)** A graph where the circle represents the mean and the tails/error bars represent the standard deviation (SD) of the H3K36me3 signal of the five different tissues. (Forebrain – Heart, Lung: p>0,05), (Hindbrain – Heart, Lung: p>0,05), (Midbrain – Heart, Lung: p>0,05). 456 bases analyzed in (B) and (D). **(C)** The changes in inclusion levels over development, adapted from Cortexa (Weißbach et al., 2024). **(D)** Graph of H3K36me3 signal of the three brain regions from Age E14.5 to P0, where the circle represents the mean, and the error bars represent the SD (B and D, quantified region: chr13:54,596,823-54,597,278 | NM_028870). P value: 0.00781 (FbP0 - FbE14.5). (HbP0 – HbE14.5: p>0,05), (MbP0 – MbE14.5: p>0,05). P-values: * < 0.05, ** < 0.01, *** < 0.001. Graphs without indicated significance indicate a lack of significant differences.

Next, Exon 5 of Cltb also exhibited differential splicing, where neurons exclusively included it, which was concordant with the exon 5-containing isoform being neuron-specific in mice (Das et al., 2021b). Specifically, the PSIs were 87.8% in the neuron, 0.0680% in the hepatocytes, and 0.794% in the lung endothelia. Both flanking exons are comparably expressed in all tissues. Peaks were noticeable in the quantified regions of the hindbrain, liver, and lung. (Fig. 5A) Further quantification evinced the lack of significant differences between the tissues' trimethylation signatures. The forebrain and midbrain had markedly smaller standard deviations, which suggested that they did not contain peaks in the region. (Fig. 5B) When we next asked if Exon 5 was developmentally regulated, we found two significant differences in inclusion in the analyzed timeframe of E14 to P0, increasing from 17.5% to 30.7% from E14 to E16 and from 30.7% to 38.5% from E16 to P0. (Fig. 5C) Subsequent quantification demonstrated a significant difference between the H3K36me3 signature of E14.5 and P0 Forebrain, an increase with age, while the hind and midbrain showed no significance. (Fig. 5D)

2.6. Mutually exclusive exons 9 and 10 of Pkm are differentially spliced in neurons

Exons 9 and 10 of Pkm (Pkm1 and 2, respectively) were mutually exclusive and exhibited differential splicing, where the neuron and cardiac muscle tended to include Exon 9 preferentially (PSIs expressed as (Exon 9 PSI, Exon 10 PSI) were (74.7%, 13.1%) and (84.1% vs 4.23%), respectively), while the lung endothelia appeared to prefer inclusion of Exon 10 (PSI (14.3% vs 62.7%)). The sole inclusion of exon 9 forms the isoform Pkm1, which was more commonly found in the brain and heart (Li et al., 2024), compared to the counterpart Pkm2, which exclusively includes exon 10, which enhances tumorigenesis and has been found elevated in lung adenocarcinoma (Zhu et al., 2021). The trimethylation tracks display larger peaks in the quantified region of Exon 9 than in Exon 10. (Fig. 6A) In analyzing both exons, we found no significant differences in either, although the lung appeared to have a smaller signal than both the neuron and cardiac muscle. (Fig. 6B & 6C) Following this, we examined whether these exons were developmentally regulated. The event saw two significant changes in preference for inclusion with age from E14 to P0. Specifically, Exon 9 inclusion was increasingly preferred with age (34.5% to 67.5% to 81.6% from E14 to E16 to P0), while Exon 10 inclusion preference decreased by equal proportions. (Fig. 6D) Additional quantification of the trimethylation signature indicated the absence of significant differences in the region of Exon 9, but also a significant difference and decrease in H3K36me3 from E14 to P0 Midbrain. The other regions did not signify any significant changes in Exon 10, however. (Fig. 6E & 6F)

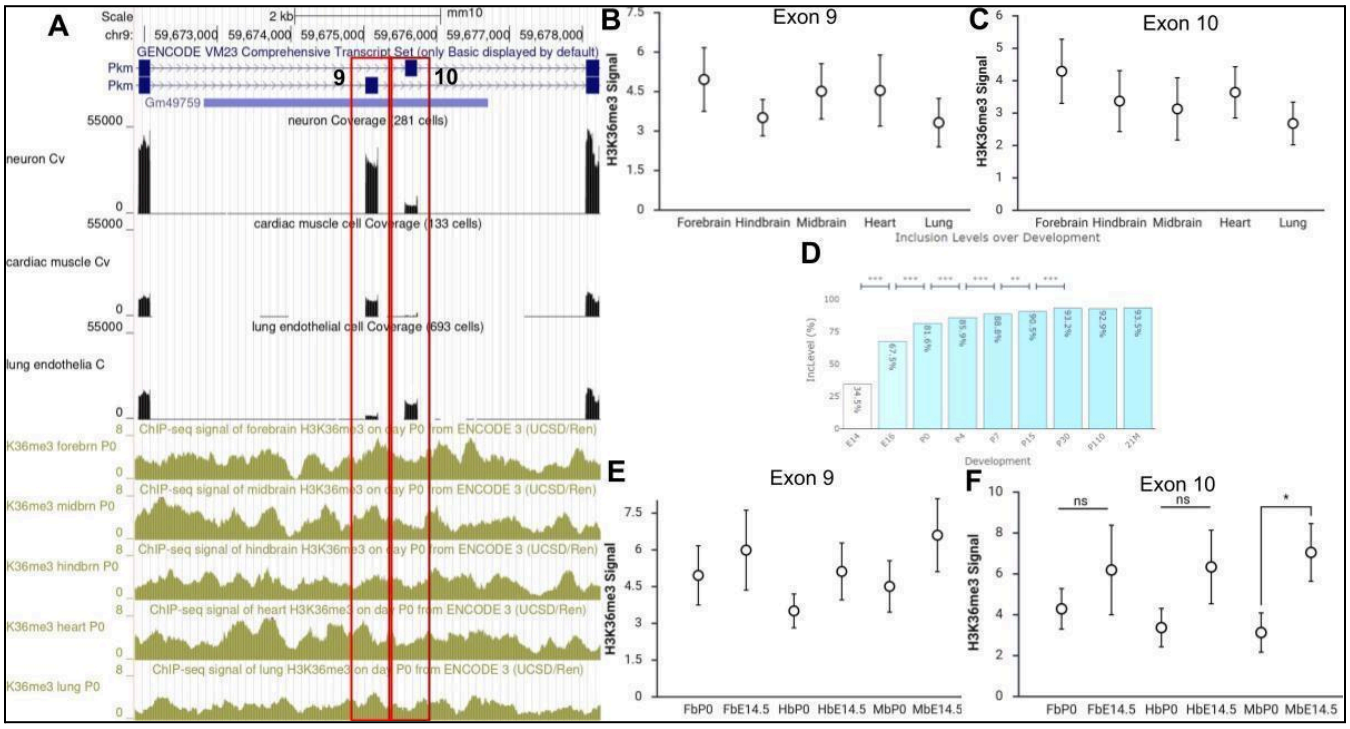

Figure 6: mRNA and H3K36me3 and alternative splicing analyses in Pkm Exons 9 and 10.

Note: **(A)** The RNA-Seq data of neurons (281 cells), cardiac muscle (133 cells), and lung endothelia (693 cells) visualized along with the associated tissues' H3K36me3 signals. **(B and C)** Graphs where the circle represents the mean and the tails/error bars represent the standard deviation (SD) of the H3K36me3 signal of the five different tissues. (Forebrain – Heart, Lung: p>0,05), (Hindbrain – Heart, Lung: p>0,05), (Midbrain – Heart, Lung: p>0,05). 570 bases analyzed in (B, C) and (E, F). **(D)** The changes in inclusion levels over development, adapted from Cortexa (Weißbach et al., 2024). In this instance, the percentages are calculated such that the percentage inclusion of exon 9 (shown above) and the percentage inclusion of exon 10 add up to 100%. **(E and F)** Graph of H3K36me3 signal of the three brain regions from Age E14.5 to P0, where the circle represents the mean, and the error bars represent the SD (B, C, E and F, Quantified regions: Exon 9: chr9:59,674,826-59,675,395, Exon 10: chr9:59,675,364-59,675,930 | NM_011099). P value: 0.0164 (MbP0 - MbE14.5). (FbP0 – FbE14.5: p>0,05), (HbP0 – HbE14.5: p>0,05), (MbP0 – MbE14.5: p>0,05). P-values: * < 0.05, ** < 0.01, *** < 0.001. Graphs without indicated significance indicate a lack of significant differences.

4. Discussion

To understand the co-regulation of H3K36me3 and alternative splicing, we investigated four genes. Our findings suggest that differences in splicing across tissues for neurally regulated alternative splicing events may be, in part, regulated by H3K36me3 in Bin1, but less so in other genes. Tissue-specific splicing of Bin1, correlated to H3K36me3 and not Mef2a or Cltb, was consistent with the literature (Forn et al., 2013; Sharma et al., 2014; Shindo et al., 2013). This tissue-specific

difference in H3K36me3 presence could potentially lead to further analysis of non-neural regulation of alternative splicing to uncover targets to modulate, influence, and reduce aberrant splicing in Alzheimer's brain tissues.

Pkm2 was known to be affected by H3K36me3 in PNT2 cells compared to hMSCs, yet it did not appear to be a major factor for tissue-specific splicing (Luco et al., 2010). This discrepancy may be due to how we quantified the H3K36me3 signals for the region containing the mutually exclusively spliced exons, while they compared the signal for upstream exons and introns as well. Otherwise, different factors, such as nucleosome occupancy, histone variants, and chromatin remodelling complexes, could be more significant components that affect splicing outcome across organs. However, this study only indicated correlations; thus, perturbation experiments are recommended to further understand H3K36me3's role in alternative splicing in interesting cases such as Bin1, as well as its potential functions in inter-tissue communication in regard to splicing.

There was no evidence of H3K36me3 being correlated with changes in developmental splicing outcomes in Bin1 and Mef2a, although it was in Cltb and Pkm. However, Cltb and Pkm both had greater developmental changes in splicing than Bin1 and Mef2a (an increase of 21% and 47.1% against 14.7% and 19.1%, respectively) and significantly increased from E14 to E16 and from E16 to P0, while Bin1 and Mef2a did not. Thus, we hypothesize that changes in H3K36me3 may be associated with a threshold for changes in splicing outcome, which could be a potential analysis in future investigations. The observation in Cltb was supported, as Cltb was known to be regulated by alternative splicing in a developmental stage-specific manner (Blue et al., 2018). The correlation was also corroborated by previous literature in mouse tissue (Hu et al., 2020). However, this study was also based on predictions and data analysis; thus, we once again recommend that experiments be carried out to examine this relationship. Furthermore, as the Cortexa database used only covers neural alternative splicing events, similar research in other tissues and organs may also be fruitful. However, splicing, being known to affect the chromatin landscape in bilateral communications, could complicate the directionality of the relationship (Yustis et al., 2024).

A limitation of this research was that, although H3K36me3 was typically known to enhance exon inclusion, there are modifications that were known to silence exons (Shindo et al., 2013; Zhou et al., 2014). These were not able to be accounted for due to time and technological constraints; however, this could have also been affecting the splicing outcome by being increased or removed between tissues instead of H3K36me3 or through various combinations of them that were known to affect differential splicing (Chen et al., 2019). For example, Mef2a is a primary downstream target of the calcium-CaMKII/PKD-HDAC pathway, which can phosphorylate histones and cause hyperacetylation that could possibly affect Mef2a splicing instead of H3K36me3 (Sharma et al., 2014). Similarly, Cltb regulation across normal tissue to adenomas was associated with a change in H3K4me3 and H3K27me3 (Forn et al., 2013), and H2BK12ac, H4K5ac, and H3K4me3 were enriched in Bin1 exon regions in IMR90 cells (Shindo et al., 2013).

The transcriptional elongation speed of RNAP II could have also affected the splicing patterns, but they could not be accounted for in this study (Zhou et al., 2014). Lastly, the methylation data were not cell-specific, so perturbation experiments could be difficult to accurately perform.

The research on two cases of correlation between developmental alternative splicing and H3K36me3 may hopefully drive experimental studies. This could then illuminate H3K36me3 as a potential target of aberrant alternative splicing during development. Specifically, it could potentially address errors in embryo growth, as it is known that embryo growth

retardation is likely caused by Pkm1 increase and Pkm2 decrease, as Pkm2 was highly expressed in embryos and essential for embryo development (Lin et al., 2021).

5. Conclusion

This study added evidence for H3K36me3's potential for altering differential splicing across tissues in Bin1, while suggesting that other factors, in part, act as key contributors for future investigations, and uncovered two cases where differences in H3K36me3 were associated with differences in developmental splicing in this investigation of histone modifications' effects on differential splicing. Although there were certain constraints, such as counter-balancing modifications and elongation speed of RNAP II, perturbation experiments could fully uncover the connections between H3K36me3, tissue-specific and developmental splicing that were previously underexplored, which could drive further investigation of the epigenetic regulation of tissue-specific and developmental conditions. In future studies, H3K36me3 could potentially be a therapeutic target for embryo growth retardation and an avenue for resolving aberrant splicing in Alzheimer's.

6. References

Agirre, E., Oldfield, A. J., Bellora, N., Segelle, A., & Luco, R. F. (2021). Splicing-associated chromatin signatures: A combinatorial and position-dependent role for histone marks in splicing definition. *Nature Communications*, 12(1), 682. https://doi.org/10.1038/s41467-021-20979-x

Bannister, A. J., & Kouzarides, T. (2011). Regulation of chromatin by histone modifications. *Cell Research*, 21(3), 381–395. https://doi.org/10.1038/cr.2011.22

Blue, R. E., Curry, E. G., Engels, N. M., Lee, E. Y., & Giudice, J. (2018). How alternative splicing affects membrane-trafficking dynamics. *Journal of Cell Science*, 131(10), jcs216465. https://doi.org/10.1242/jcs.216465

Chang, M. Y., Boulden, J., Katz, J. B., Wang, L., Meyer, T. J., Soler, A. P., Muller, A. J., & Prendergast, G. C. (2007). Bin1 Ablation Increases Susceptibility to Cancer during Aging, Particularly Lung Cancer. *Cancer Research*, 67(16), 7605–7612. https://doi.org/10.1158/0008-5472.CAN-07-1100

Chen, W., Song, X., & Lin, H. (2019). Combinatorial Pattern of Histone Modifications in Exon Skipping Event. *Frontiers in Genetics*, 10. https://doi.org/10.3389/fgene.2019.00122

Chou, M.-Y., Underwood, J. G., Nikolic, J., Luu, M. H. T., & Black, D. L. (2000). Multisite RNA Binding and Release of Polypyrimidine Tract Binding Protein during the Regulation of c-src Neural-Specific Splicing. *Molecular Cell*, 5(6), 949–957. https://doi.org/10.1016/S1097-2765(00)80260-9

Das, J., Tiwari, M., & Subramanyam, D. (2021a). Clathrin Light Chains: Not to Be Taken so Lightly. *Frontiers in Cell and Developmental Biology*, 9, 774587. https://doi.org/10.3389/fcell.2021.774587

Das, J., Tiwari, M., & Subramanyam, D. (2021b). Clathrin Light Chains: Not to Be Taken so Lightly. *Frontiers in Cell and Developmental Biology*, 9, 774587. https://doi.org/10.3389/fcell.2021.774587

De Jager, P., Srivastava, G., Lunnon, K., Burgess, J., Schalkwyk, L., Yu, L., Eaton, M., Keenan, B., Ernst, J., McCabe, C., Tang, A., Raj, T., Replogle, J., Brodeur, W., Gabriel, S., Chai, H., Younkin, C., Younkin, S., Zou, F., … Bennett, D. (2014). Alzheimery's disease pathology is associated with early alterations in brain DNA methylation at ANK1, BIN1, RHBDF2 and other loci. *Nature Neuroscience*, 17(9), 1156–1163. https://doi.org/10.1038/nn.3786

de la Mata, M., Alonso, C. R., Kadener, S., Fededa, J. P., Blaustein, M., Pelisch, F., Cramer, P., Bentley, D., & Kornblihtt, A. R. (2003). A Slow RNA Polymerase II Affects Alternative Splicing In Vivo. *Molecular Cell*, 12(2), 525–532. https://doi.org/10.1016/j.molcel.2003.08.001

Dourlen, P., Kilinc, D., Landrieu, I., Chapuis, J., & Lambert, J.-C. (2025). BIN1 and Alzheimer's disease: The tau connection. *Trends in Neurosciences*, 48(5), 349–361. https://doi.org/10.1016/j.tins.2025.03.004

Ellis, J. D., Barrios-Rodiles, M., Çolak, R., Irimia, M., Kim, T., Calarco, J. A., Wang, X., Pan, Q., O'Hanlon, D., Kim, P. M., Wrana, J. L., & Blencowe, B. J. (2012). Tissue-Specific Alternative Splicing Remodels Protein-Protein Interaction Networks. *Molecular Cell*, 46(6), 884–892. https://doi.org/10.1016/j.molcel.2012.05.037

ENCODE Project Consortium. (2012). An integrated encyclopedia of DNA elements in the human genome. *Nature*, 489(7414), 57–74. https://doi.org/10.1038/nature11247

Forn, M., Muñoz, M., Tauriello, D. V. F., Merlos-Suárez, A., Rodilla, V., Bigas, A., Batlle, E., Jordà, M., & Peinado, M. A. (2013). Long range epigenetic silencing is a trans-species mechanism that results in cancer specific deregulation by overriding the chromatin domains of normal cells. *Molecular Oncology*, 7(6), 1129–1141. https://doi.org/10.1016/j.molonc.2013.08.008

Georgopoulos, K. (2017). In search of the mechanism that shapes the neutrophil's nucleus. *Genes & Development*, 31(2), 85–87. https://doi.org/10.1101/gad.296228.117

Greer, E. L., & Shi, Y. (2012). Histone methylation: A dynamic mark in health, disease and inheritance. *Nature Reviews. Genetics*, 13(5), 343–357. https://doi.org/10.1038/nrg3173

Hu, Q., Greene, C. S., & Heller, E. A. (2020). Specific histone modifications associate with alternative exon selection during mammalian development. *Nucleic Acids Research*, 48(9), 4709–4724. https://doi.org/10.1093/nar/gkaa248

Irimia, M., Weatheritt, R. J., Ellis, J., Parikshak, N. N., Gonatopoulos-Pournatzis, T., Babor, M., Quesnel-Vallières, M., Tapial, J., Raj, B., O'Hanlon, D., Barrios-Rodiles, M., Sternberg, M. J. E., Cordes, S. P., Roth, F. P., Wrana, J. L., Geschwind, D. H., & Blencowe, B. J. (2014). A highly conserved program of neuronal microexons is misregulated in autistic brains. *Cell*, 159(7), 1511–1523. https://doi.org/10.1016/j.cell.2014.11.035

Leung, C. S., Douglass, S. M., Morselli, M., Obusan, M. B., Pavlyukov, M. S., Pellegrini, M., & Johnson, T. L. (2019a). H3K36 Methylation and the Chromodomain Protein Eaf3 Are Required for Proper Cotranscriptional Spliceosome Assembly. *Cell Reports*, 27(13), 3760-3769.e4. https://doi.org/10.1016/j.celrep.2019.05.100

Leung, C. S., Douglass, S. M., Morselli, M., Obusan, M. B., Pavlyukov, M. S., Pellegrini, M., & Johnson, T. L. (2019b). H3K36 Methylation and the Chromodomain Protein Eaf3 Are Required for Proper Cotranscriptional Spliceosome Assembly. *Cell Reports*, 27(13), 3760-3769.e4. https://doi.org/10.1016/j.celrep.2019.05.100

Li, Y., Zhang, S., Li, Y., Liu, J., Li, Q., Zang, W., & Pan, Y. (2024). The Regulatory Network of hnRNPs Underlying Regulating PKM Alternative Splicing in Tumor Progression. *Biomolecules*, 14(5), 566. https://doi.org/10.3390/biom14050566

Lin, J., Wu, S., Shen, Q., Liu, J., Huang, S., Peng, G., & Qiao, Y. (2021). Base editing-mediated perturbation of endogenous PKM1/2 splicing facilitates isoform-specific functional analysis in vitro and in vivo. *Cell Proliferation*, 54(8), e13096. https://doi.org/10.1111/cpr.13096

Luco, R. F., Allo, M., Schor, I. E., Kornblihtt, A. R., & Misteli, T. (2011). Epigenetics in Alternative Pre-mRNA Splicing. *Cell*, 144(1), 16–26. https://doi.org/10.1016/j.cell.2010.11.056

Luco, R. F., Pan, Q., Tominaga, K., Blencowe, B. J., Pereira-Smith, O. M., & Misteli, T. (2010). Regulation of Alternative Splicing by Histone Modifications. *Science (New York, N.Y.)*, 327(5968), 996–1000. https://doi.org/10.1126/science.1184208

Marasco, L. E., & Kornblihtt, A. R. (2023). The physiology of alternative splicing. *Nature Reviews. Molecular Cell Biology*, 24(4), 242–254. https://doi.org/10.1038/s41580-022-00545-z

Montes, M., Sanford, B. L., Comiskey, D. F., & Chandler, D. S. (2019). RNA splicing and disease: Animal models to therapies. *Trends in Genetics : TIG*, 35(1), 68–87. https://doi.org/10.1016/j.tig.2018.10.002

Nakamura, Y. (1994). Involvement of clathrin light chains in the pathology of Alzheimer's disease. *Acta Neuropathologica*, 87(1), 23–31. https://doi.org/10.1007/BF00386251

Nakamura, Y., Takeda, M., Yoshimi, K., Hattori, H., Hariguchi, S., Hashimoto, S., & Nishimura, T. (1994). Involvement of clathrin light chains in the pathology of Pick's disease; impilication for impairment of axonal transport. *Neuroscience Letters*, 180(1), 25–28. https://doi.org/10.1016/0304-3940(94)90905-9

Nutter, C. A., Jaworski, E. A., Verma, S. K., Deshmukh, V., Wang, Q., Botvinnik, O. B., Lozano, M. J., Abass, I. J., Ijaz, T., Brasier, A. R., Garg, N. J., Wehrens, X. H. T., Yeo, G. W., & Kuyumcu-Martinez, M. N. (2016). Dysregulation of RBFOX2 is an early event in cardiac pathogenesis of diabetes. *Cell Reports*, 15(10), 2200–2213. https://doi.org/10.1016/j.celrep.2016.05.002

Okamoto, S., Nakamura, T., Cieplak, P., Chan, S. F., Kalashnikova, E., Liao, L., Saleem, S., Han, X., Clemente, A., Nutter, A., Sances, S., Brechtel, C., Haus, D., Haun, F., Sanz-Blasco, S., Huang, X., Li, H., Zaremba, J. D., Cui, J., … Lipton, S. A. (2014). S-Nitrosylation-Mediated Redox Transcriptional Switch Modulates Neurogenesis and Neuronal Cell Death. *Cell Reports*, 8(1), 217–228. https://doi.org/10.1016/j.celrep.2014.06.005

Passier, R., Zeng, H., Frey, N., Naya, F. J., Nicol, R. L., McKinsey, T. A., Overbeek, P., Richardson, J. A., Grant, S. R., & Olson, E. N. (2000). CaM kinase signaling induces cardiac hypertrophy and activates the MEF2 transcription factor in vivo. *The Journal of Clinical Investigation*, 105(10), 1395–1406. https://doi.org/10.1172/JCI8551

Perez, G., Barber, G. P., Benet-Pages, A., Casper, J., Clawson, H., Diekhans, M., Fischer, C., Gonzalez, J. N., Hinrichs, A. S., Lee, C. M., Nassar, L. R., Raney, B. J., Speir, M. L., van Baren, M. J., Vaske, C. J., Haussler, D., Kent, W. J., & Haeussler, M. (2025). The UCSC Genome Browser database: 2025 update. *Nucleic Acids Research*, 53(D1), D1243–D1249. https://doi.org/10.1093/nar/gkae974

Pfluger, J., & Wagner, D. (2007). Histone modifications and dynamic regulation of genome accessibility in plants. *Current Opinion in Plant Biology*, 10(6), 645–652. https://doi.org/10.1016/j.pbi.2007.07.013

Piovesan, A., Pelleri, M. C., Antonaros, F., Strippoli, P., Caracausi, M., & Vitale, L. (2019). On the length, weight and GC content of the human genome. *BMC Research Notes*, 12, 106. https://doi.org/10.1186/s13104-019-4137-z

Schaum, N., Karkanias, J., Neff, N. F., May, A. P., Quake, S. R., Wyss-Coray, T., Darmanis, S., Batson, J., Botvinnik, O., Chen, M. B., Chen, S., Green, F., Jones, R. C., Maynard, A., Penland, L., Pisco, A. O., Sit, R. V., Stanley, G. M., Webber, J. T., … Principal investigators. (2018). Single-cell transcriptomics of 20 mouse organs creates a Tabula Muris. *Nature*, 562(7727), 367–372. https://doi.org/10.1038/s41586-018-0590-4

Sharma, A., Nguyen, H., Geng, C., Hinman, M. N., Luo, G., & Lou, H. (2014). Calcium-mediated histone modifications regulate alternative splicing in cardiomyocytes. *Proceedings of the National Academy of Sciences of the United States of America*, 111(46), E4920–E4928. https://doi.org/10.1073/pnas.1408964111

Shindo, Y., Nozaki, T., Saito, R., & Tomita, M. (2013). Computational analysis of associations between alternative splicing and histone modifications. *FEBS Letters*, 587(5), 516–521. https://doi.org/10.1016/j.febslet.2013.01.032

Spooner, H. C., & Dixon, R. E. (2025). Bend it Like BIN1: How a Membrane-Curving Adaptor Protein Shapes Cardiac Physiology. *American Journal of Physiology. Heart and Circulatory Physiology*, 329(1), H94–H108. https://doi.org/10.1152/ajpheart.00198.2025

Weißbach, S., Milkovits, J., Pastore, S., Heine, M., Gerber, S., & Todorov, H. (2024). Cortexa: A comprehensive resource for studying gene expression and alternative splicing in the murine brain. *BMC Bioinformatics*, 25(1), 293. https://doi.org/10.1186/s12859-024-05919-y

Wright, C. J., Smith, C. W. J., & Jiggins, C. D. (2022). Alternative splicing as a source of phenotypic diversity. *Nature Reviews. Genetics*, 23(11), 697–710. https://doi.org/10.1038/s41576-022-00514-4

Xu, Y., Zhao, W., Olson, S. D., Prabhakara, K. S., & Zhou, X. (2018). Alternative splicing links histone modifications to stem cell fate decision. *Genome Biology*, 19(1), 133. https://doi.org/10.1186/s13059-018-1512-3

Yustis, J.-C., Devoucoux, M., & Côté, J. (2024). The Functional Relationship Between RNA Splicing and the Chromatin Landscape. *Journal of Molecular Biology*, 436(16), 168614. https://doi.org/10.1016/j.jmb.2024.168614

Zhang, Q., Wang, S.-S., Zhang, Z., & Chu, S.-F. (2025). PKM2-mediated metabolic reprogramming of microglia in neuroinflammation. *Cell Death Discovery*, 11(1), 149. https://doi.org/10.1038/s41420-025-02453-5

Zhou, H.-L., Luo, G., Wise, J. A., & Lou, H. (2014). Regulation of alternative splicing by local histone modifications: Potential roles for RNA-guided mechanisms. *Nucleic Acids Research*, 42(2), 701–713. https://doi.org/10.1093/nar/gkt875

Zhu, H., Li, T., Shi, S., Chen, D., Chen, W., & Chen, H. (2021). ESCO2 promotes lung adenocarcinoma progression by regulating hnRNPA1 acetylation. *Journal of Experimental & Clinical Cancer Research : CR*, 40, 64. https://doi.org/10.1186/s13046-021-01858-1

Data & Code Availability Statement

The following publicly available databases were used in this study.

- TabulaMurisSingleCellData: https://genome.ucsc.edu/cgi-bin/hgTrackUi?hgsid=2303618686_hFf8vDaGo1RWvlEehhPpGvHhSniv&db=mm10&c=chr2&g=tabulaMuris
- ChIP-Seq: https://www.encodeproject.org/chip-seq/histone-encode3/
- Bin1: https://genome.ucsc.edu/s/RWucscgb/mm10_H3K36me3_RNA%2DSeq_UCSC_Bin1_AllOrgans_FigureV1
- Mef2a: https://genome.ucsc.edu/s/RWucscgb/mm10_H3K36me3_RNA%2DSeq_UCSC_Mef2a_AllOrgans_FigureV1
- Cltb: https://genome.ucsc.edu/s/RWucscgb/mm10_H3K36me3_RNA%2DSeq_UCSC_Cltb_AllOrgans_FigureV1
- Pkm: https://genome.ucsc.edu/s/RWucscgb/mm10_H3K36me3_RNA%2DSeq_UCSC_Pkm_AllOrgans_FigureV1
- Cortexa: https://cortexa-01.zdv.uni-mainz.de/

Acknowledgements

Special thanks to **Kif Liakath-Ali** for his mentoring and supervision of this project. I thank my family who have supported me in writing this paper. I thank Indigo Research for allowing me to write an empirical article. I thank the developers and contributors of the Cortexa database, the UCSC Genome Browser, and the ENCODE project for their data and visualisation tools. All figures in this manuscript were made with the help of BioRender.

Author Biography

Ryota Watanabe is a 16-year-old student researcher of chromatin biology at Crimson Global Academy in Nishinomiya City, Japan. Inspired by the immense compaction in DNA packaging, he enjoys investigating the mechanisms of chromatin regulation through epigenetics. Additionally, he hopes to apply his theoretical research to improving the lives of the rare disease community and runs an educational YouTube channel about rare diseases. He hopes to major in molecular biology at the university.

Mentor Contribution Statement

The mentor for this research project was **Dr Kif Liakath-Ali**. He served as the sole supervisor throughout the work. He met with the author weekly via Zoom to provide guidance, discuss progress, and offer critical feedback. He recommended relevant databases for analysis, which the author independently explored and interrogated. Dr Liakath-Ali reviewed the data analysis and read multiple drafts of the manuscript to identify issues of logic, clarity, or sophistication; however, all analyses, interpretations, and written materials were prepared entirely by the author.